Runaway electron studies in TEXTOR

2015 Nucl. Fusion 55 053008

(http://iopscience.iop.org/0029-5515/55/5/053008)

OPEN ACCESS
IOP Publishing | International Atomic Energy Agency Nuclear Fusion
Nucl. Fusion **55** (2015) 053008 (12pp) doi:10.1088/0029-5515/55/5/053008

Runaway electron studies in TEXTOR

K. Wongrach[1], K.H. Finken[1], S.S. Abdullaev[2], O. Willi[1], L. Zeng[3], Y. Xu[4] and the TEXTOR Team

[1] Institut für Laser-und Plasmaphysik, Heinrich-Heine Universität Düsseldorf, Germany
[2] Institut für Energie-und Klimaforschung, Forschungszentrum Jülich GmbH, Jülich, Germany
[3] Institute of Plasma Physics, Chinese Academy of Sciences, Hefei, People's Republic of China
[4] Southwestern Institute of Physics, Chengdu, People's Republic of China

E-mail: kunaree.wongrach@uni-duesseldorf.de

Received 23 October 2014, revised 19 February 2015
Accepted for publication 26 February 2015
Published 15 April 2015

Abstract

The evolution of runaway electrons in disruptive plasmas in TEXTOR is determined by observing the synchrotron radiation (hard component $E > 25$ MeV) and by measuring the runway electrons with an energy of a few MeV using a scintillator probe. Disruptions are initiated by a massive argon gas injection performed by a fast valve. The observed runaway beam of the high energy component (synchrotron radiation) fills about half of the diameter of the original plasma. The beam is smooth and shows no indication of filamentation. The initial conditions are in all cases very similar. The temporal development of the runaway electrons, however, is different: one observes cases with and without subsequent mode excitation and other cases in which the hard runaway component survives the apparent end of the runaway plateau. Several methods are applied to remove the runaway electrons including massive gas injection from two additional valves of different sizes as well as external and internal ergodization by inducing a tearing mode. The mitigation is only marginally successful and it is clearly found that the runaways in disruptions are substantially more robust than runaways created in stationary, low density discharges.

Keywords: runaway, mitigation, disruption, TEXTOR, tokamak

(Some figures may appear in colour only in the online journal)

1. Introduction

During a disruption, a sudden loss of magnetic confinement, the energy stored in the plasma is rapidly lost to the plasma facing components (PFCs) [1]. The damage to the machine following the disruption is caused by: (a) the transient heat load during the thermal quench (TQ), (b) the high forces applied to the PFCs and the vessel resulting from the halo and eddy currents, and (c) the energetic runaway electrons (REs). Several methods have been proposed in order to mitigate the effects of disruptions. It has been shown in several tokamaks that the damaging effects of disruptions are significantly reduced by early injection of impurity species [2]. Killer pellet injection is one of the methods for rapid insertion of impurities into a tokamak plasma. Experiments on disruption mitigation by using pellets of neon, argon and methane have been performed in several tokamaks [3–6]. The pellet increases the radiated power and reduces the mechanical loads on the vessel wall by up to 50%, the thermal flux on the divertor by 25–40%, and the peak halo current by 50%. Nevertheless, the production of REs has been caused also by the pellet injection [5, 6]. Another potential candidate for disruption mitigation is a massive gas injection [7]. A gas injection system creates a subsonic gas jet which delivers a large quantity of neutral gas ($>10^{22}$ atoms) into the vacuum vessel within $\leqslant 5$ ms [8]. The rapid shutdown by puffing noble gases, e.g. helium, neon or argon, in JET [9], ASDEX upgrade [10], DIII-D [11], Tore-Supra [12], JT-60U [13] and TEXTOR [14] demonstrates the mitigation of the halo current and the significant reduction of the heat load during TQ by enhanced radiation. Massive helium injection effectively suppresses REs [12]. Argon injection, in contrast, is prone to runaway generation. However, the TEXTOR disruptions initiated by argon injection can become runaway free if the number of atoms exceeds $14 \pm 2 \times 10^{21}$, i.e. around 140 times the plasma electron content [14]. Additionally, the injection of mixtures of argon with hydrogen [13] or deuterium [14] also provides runaway-free disruptions.

Several experiments have been dedicated to the study of runaway generation and suppression during disruptions in different tokamaks [14–16]. Most studies of runaway mitigation concentrate on a massive gas injection. In next-generation tokamaks such as ITER, REs with energies of the order of a few hundred MeV are expected [17]. In order

to avoid runaway generation during ITER disruptions, either 1.5×10^{25} molecules of helium gas or 1.8×10^{24} molecules of argon gas have to be delivered within a few milliseconds [18]. This requirement cannot be achieved by the present-day devices. Moreover, the injection of a large amount of gas may affect the vacuum system. It has been shown in [19] that a fast gas puff with a moderate amount of helium leads to the loss of the existing REs and the plasma current decay time is shortened. Magnetic perturbations are another method applied to mitigate the REs. The suppression of the runaway avalanche during TEXTOR disruptions is observed when a perturbation field with $n = 1$ and $n = 2$ is applied [20].

In this paper, we present initially some examples of the evolution of runaways without additional mitigation methods and then a systematic study of different runaway mitigation methods used in TEXTOR including a gas puff and mitigation by the dynamic ergodic divertor (DED). The mitigation approaches are applied to disruptions initiated by a fast argon puff. The paper focuses in particular on the observation of the IR-synchrotron radiation which is sensitive to runaways with energies $E_r \gtrsim 25$ MeV and the measurement of the runaway probe which is sensitive to runaways leaving the plasma with energies between 3.5 and 22 MeV. An overview of the different observations detected by these diagnostics is given.

2. Experimental Setup

The experimental measurements were carried out in TEXTOR (a tokamak with circular cross section, $R_0 = 1.75$ m, $a = 0.46$ m) operated in a pure ohmic mode without additional heating. The discharge conditions are: toroidal field: $B_T = 2.4$ T, plasma current: $I_P = 350$ kA and line average central density: $n_e = 1.5 \times 10^{19}$ m^{-3}. When the discharge is in the steady state condition, i.e. 2 s after the start of the discharge, 9.7×10^{20} atoms of argon are injected in order to trigger a disruption in a reproducible way. Beyond the standard diagnostics of TEXTOR the following diagnostics and equipment are used: an infrared (IR) camera for observing the synchrotron radiation from highly relativistic electrons, a runaway probe for energetic electrons leaving the plasma, different fast valves for initiating disruptions and for mitigating the runaways created during the disruptions, and the ergodization system of TEXTOR (the DED) for possibly reducing the runaway damage at the walls.

2.1. The IR detection system

An IR camera is used to observe the synchrotron radiation emitted by the REs. It is located of the equatorial mid-plane of TEXTOR. The camera is oriented to the direction of electron approach such that it is sensitive to the synchrotron radiation of REs. Its field of view covers the low field side (LFS) of the torus. The camera is sensitive for wavelengths between 3 and 5 μm. It is operated at a frame rate of 1253 frames per second with an integration time of 2 μs. Since the REs emit synchrotron radiation into the forward direction with a small opening angle, the camera detects the confined REs with energies higher than 25 MeV only from the area where the orbit of the runaways is directed towards the entrance lens of the IR optics. Analysis of synchrotron radiation has been described in detail elsewhere [21].

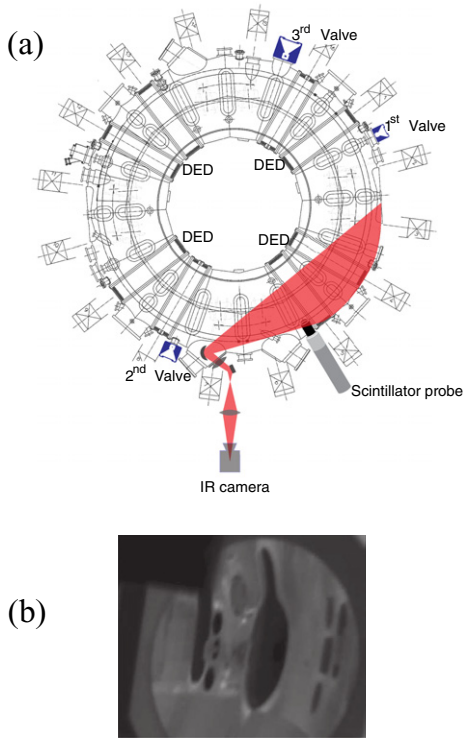

Figure 1. (*a*) Schematic top view of TEXTOR with the experimental setup for the measurements of REs. Three fast valves are located at different positions. The scintillator probe is inserted from the LFS of the torus at the equatorial plan. The synchrotron radiation as well as the IR radiation from other sources are collected and directed to an IR camera. The red area presents the camera field of view. (*b*) The camera view: openings for windows and diagnostic ports on the liner are clearly seen.

In addition, the camera measures also the thermal radiation of the wall components. A view of the wall, heated up to 150 °C without plasma, is shown in figure 1(*b*). One clearly sees the liner with openings for windows and diagnostic ports. The background thermal objects enable the reconstruction of the location from where the synchrotron radiation is emitted. Details of observation of synchrotron radiation have recently been reported in [22]. The structure and dynamics of the runaway beam have been observed.

2.2. Scintillator probe

A scintillator probe measures the REs at the plasma edge. The probe is inserted from the LFS shortly before the disruption is triggered and remains at the edge of the plasma at the minor radius $a = 0.46$ m until the plasma termination. Only the REs with energies exceeding 3.5 MeV can penetrate through the CFC housing and reach the scintillating crystals inside the probe. The probe consists of nine scintillating crystals connected via glass fibre cables to photomultipliers. Each crystal measures the REs at a different energy range; the probe is sensitive in an energy range between 3.5 and 22 MeV. The details of the probe are described in [23].

2.3. The valves

TEXTOR is equipped with three fast valves [24]. The valves are activated by an eddy current, which is induced by a current

Table 1. Characteristics of the valves at TEXTOR—orifice diameter, volume, maximum operating pressure and location of the valves.

Valve	$Ø_{\text{orifice}}(mm)$	Vol (cm^3)	P_{max} (MPa)	Location
1	8	20	3.2	top of TEXTOR
2	14	30	3.0	equatorial plane
3	28	110	15	equatorial plane

flowing in a pancake-type coil. Since the valves do not contain any ferrite materials, they can be installed very close to or even inside the vacuum vessel with its full magnetic field. The characteristics of these valves are shown in table 1. Valve 1 has been installed in order to create and study disruptions. Its gas flow has been characterized by a Michelson interferometer in the downstream flow of a guiding vacuum tube [25]. The flow rate and, in particular, the front of the gas are limited by a valve orifice of 8 mm and by the guiding tube length and diameter. If the valve is filled with 0.2 MPa of argon, disruptions with runaway generation are produced reproducibly. The gas reservoir volume of the valve amounts to 250 cm^3; however here it is reduced by an insert to 20 cm^3 only.

Valve 2 has a gas reservoir of 30 cm^3. Only half of the gas in the reservoir is released because the valve closes quickly after the activation. The valve is mounted close to the plasma such that there is only a small delay in the flow. Previously, even a smaller valve has successfully been applied to expel REs from a low density discharge [26]. The valve was operated with helium gas. After the gas injection, the REs were expelled even before the TQ took place. One aim of the following experiments is to test whether the injection of such an amount of gas will also suppress the runaways created during disruptions or whether the behaviour of REs in low density discharges is different.

Valve 3 has the largest orifice such that the gas can be quickly released. The gas throughput is about an order of magnitude higher than by valve 1. It is designed for a pressure up to 3.2 MPa in order that a moderate gas reservoir provides a high amount of gas. Here only low gas pressures are used. Therefore, the volume of the gas reservoir is reduced from more than 1 dm^3 to 110 cm^3 by adding an insert, similar as in valve 1 [27]. The valve has been mounted close to the plasma inside the TEXTOR vessel such that the delay due to the gas flow is minimal.

In order to suppress the runaway generation completely by fast gas injection, an argon gas density of more than $5 \times 10^{22}\,m^{-3}$ is required [28]. This corresponds to a gas pressure in the vessel of about 0.207 kPa. In TEXTOR, the valve would have to inject 3.5×10^{23} atoms of argon. Here, valve 1 is used only to initiate runaway disruptions, while valve 2 and valve 3 are applied to suppress the REs. Valve 2 and valve 3 are mounted at a vessel flange in the equatorial plane as close to the plasma as possible. This minimizes the flow time of the gas. For technical reasons the gas path of valve 1 is 0.5 m longer. Therefore the time delay between the valve trigger and the arrival time of the gas at the plasma surface is about 2 ms longer than the time delay of the other valves [27].

2.4. Ergodization

Another approach for RE mitigation is the DED of TEXTOR. The DED is a set of magnetic perturbation coils. Sixteen individual coils and two compensation coils are wound around the torus at the high field side (HFS) following the direction of the equilibrium magnetic field lines [29]. The electrical current in the coils generates a magnetic field which is resonant to the plasma magnetic field in particular near the $q = 3$ surface. The DED coils can be connected in different ways such that the dominant base modes $m/n = 12/4$ or $m/n = 6/2$ or $m/n = 3/1$ can be excited. In addition to the base modes, also neighbouring modes are generated which lead to a cascade of magnetic islands in the plasma. If the islands are wide enough such that they overlap, the magnetic field becomes ergodic which means that a magnetic field line is not restricted to a surface but fills the whole volume. The so-called laminar zone is formed by those field lines which intersect limiters or the wall. Particles, in particular the collisionless runaways, are lost practically immediately from this area.

The radial penetration of the perturbation field B_{p} scales with about $B_{\text{p}}(r) \approxeq B_{\text{p}}(a) \cdot (\frac{r}{a})^m$; therefore, the penetration of modes with high m—numbers is very limited while the $m/n = 3/1$ penetrates deeply into the plasma. The islands resulting from the $m/n = 3/1$ base mode can be a seed for $m/n = 2/1$ tearing modes in the plasma [30]. The dynamic option, allowing for a rotation of the perturbation field, is not applied here.

3. Typical induced disruptions in TEXTOR

In order to induce a disruption, 9.7×10^{20} atoms of argon were injected by valve 1 into the plasma at $t = 2$ s after the start-up. The TQ took place when the edge of plasma up to the $q = 2$ surface had been cooled. A significant number of REs was generated during such disruptions. During all discharges presented in this section, no additional mitigation methods are applied. Under the same initial conditions, three types of disruption evolutions have been observed.

3.1. Runaway disruptions without mode excitation

The start of a disruption is characterized with respect to the IR camera by a flash of thermal radiation from the vessel wall. For the given valve and gas feeding line, this is about 4 ms after the argon injection. At this time, the wall is heated by the lost electrons and ions during the TQ (see figures 2(*A*)(*a*) and 2(*B*)(*a*)). We use this flash as the time marker of the disruption. After the REs have gained a sufficiently high energy, the RE beam becomes visible at the HFS. The width of the runaway beam in the vertical direction is about one half of the original plasma diameter. In the horizontal direction, the camera view is vignetted, therefore, we cannot see the whole beam. The RE beam then grows and moves towards the LFS. The structures which are seen in figures 2(*A*)(*b*)–(*f*) (indicated by white arrows) result from the reflection from the vessel wall. At $t = 2.032$ s, the position control system generates the magnetic fields such that the RE beam is pushed back to the HFS. As the loop voltage increases, the REs are accelerated. The intensity at the centre of the beam increases. However, the beam radius decreases. This indicates that with increasing energy, only the REs at the centre are well confined while the REs at the edge are lost.

In addition to the IR image from the IR camera, we calculate a time derivative of each IR image by subtracting

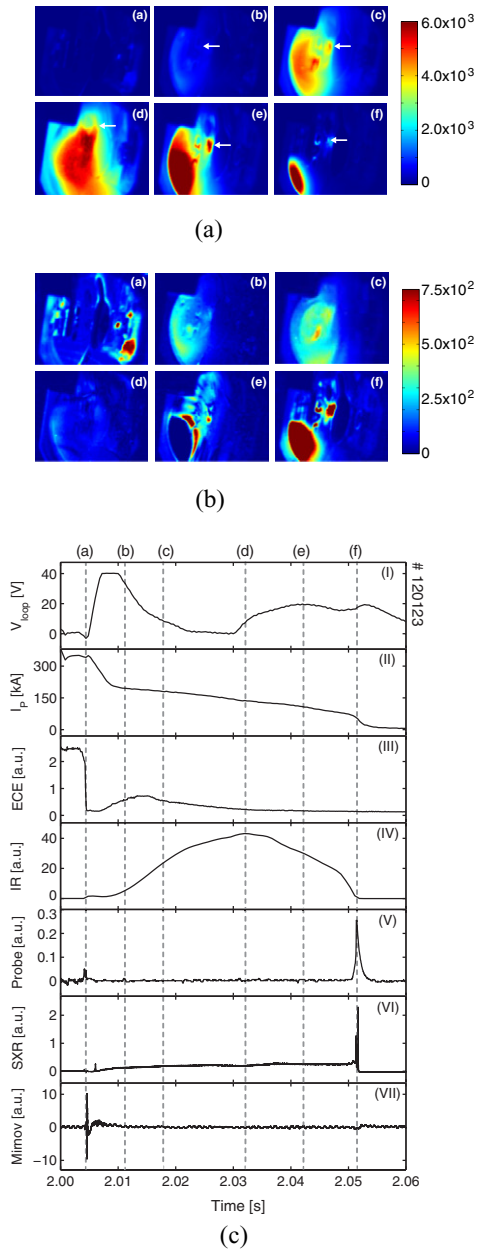

Figure 2. (*A*) IR images observed by the camera and (*B*) the images obtained from subtracting consecutive images for discharge #120123 at (*a*) $t = 2.004$ s, (*b*) $t = 2.011$ s, (*c*) $t = 2.018$ s, (*d*) $t = 2.032$ s, (*e*) $t = 3.042$ s and (*f*) $t = 2.051$ s. White arrows indicate structures from the reflection. (*C*) Temporal evolution of the disruption of discharge #120123: (top to bottom) time trace of the loop voltage, the plasma current, the ECE signal, the intensities added over all pixels of the IR image, the scintillator probe signal, the SXR signal and the Mirnov signal. Dashed lines (a)–(f) correspond to the sub-figures (*a*)–(*f*) in (*A*) and (*B*).

the image from the previous image. This representation is very sensitive to relatively small but fast variations of the RE distribution. The absolute values of consecutive image subtractions corresponding to figures 2(*A*)(*a*)–(*f*) are shown in figures 2(*B*)(*a*)–(*f*), respectively. Of particular interest is the loss phase of the REs, namely sub-figures (*e*) and (*f*). One sees that the core of the REs is hardly affected in this phase and that the loss occurs as a peeling of the RE beam edge, especially in sub-figure (*e*), a loss channel towards the top is observed.

Figure 2(*C*) shows the evolution of the characteristic signals during the disruption. Displayed from top to bottom are: the loop voltage, the plasma current, the electron cyclotron emission (ECE) signal, the integrated synchrotron radiation, the runaway probe signal, the soft x-ray (SXR) signal and the Mirnov signal. During the TQ (dashed line (*a*) in figure 2(*C*)), a negative loop voltage spike and a sudden drop of the ECE signal as well as a strong Mirnov signal oscillation are observed. A runaway burst and a SXR spike which indicate the runaway loss are consistent with the loss observed by the IR camera shown in figure 2(*A*)(*a*).

In a 'quiet' disruption such as discharge #120123, neither the SXR spikes nor Mirnov signal spikes are present during the runaway plateau phase. The level of the probe signal in figure 2(*C*)(V) is rather low with the exception of a small spike at the TQ and at the termination of the runaway plateau. The plasma current shown in figure 2(*C*)(II) decays smoothly. This confirms that the major part of REs is well confined within the plasma. A decrease in the intensities added over all pixels of the IR image shown in figure 2(*C*)(IV) is caused by the movement of the beam. At the end of the discharge, the runaway beam disappears rapidly. Sharp SXR spikes and a RE burst are observed. All REs are lost immediately.

3.2. Runaways with mode excitation

The 'quiet' disruption belongs to one class of observations. In another class, mode excitation is observed as seen, for instance, in discharge #119990. In this case, the runaway beam is located at the centre of the camera view and is not vignetted. The runaway beam becomes visible and develops at the HFS similar to the first case (see figure 3(*A*)). However, in this case the runaway beam continues moving towards LFS. The beam touches the scintillator probe and heats it up as can be seen in figures 3(*A*)(*b*)–(*f*).

Despite the increasing loop voltage shown in figure 3(*C*)(I) dashed line (c), the intensity of the beam at the centre does not change significantly. Only slight changes obtained from subtracting two consecutive images are present (see figure 3(*B*)). The runaway bursts, the SXR spikes and Mirnov signal spikes are present as can be seen in figures 3(*C*)(V)–(VII), respectively. The excitation mode created during the runaway plateau phase leads to losses and inhibits the runaway beam development.

Even though the probe signal is enhanced and the decay rate of the plasma current increases, the IR signal in (IV) varies only slightly. This indicates that the loss in the medium and low energy band is substantially higher than in the high energy band. The beginning of the mode excitation seems to be dependent on the position of the runaway beam. The mode excitation is observed when the runaway beam touches the wall or the probe. However, the mode excitation sometimes appears longer or shorter than the contact time.

Although the runaway currents in both cases are comparable, the maximum intensity of the runaway beam is about 20% lower than in the previous case. The runaway beam becomes smaller with increasing time. During the runaway plateau termination, all REs are lost. The IR signal drops

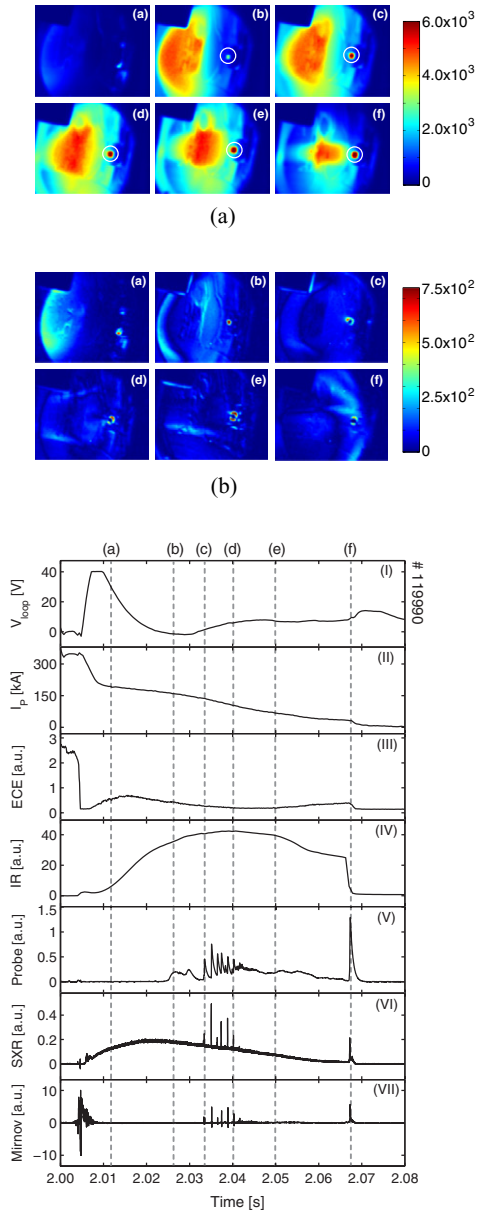

Figure 3. (*A*) IR images observed by the camera and (*B*) the images obtained from subtracting consecutive images for discharge #119990 at (*a*) $t = 2.011$ s, (*b*) $t = 2.027$ s, (*c*) $t = 2.033$ s, (*d*) $t = 2.040$ s, (*e*) $t = 3.050$ s and (*f*) $t = 2.067$ s. White rings indicate the scintillator probe tip. (*C*) Temporal evolution of the disruption of discharge #119990: (top to bottom) time trace of the loop voltage, the plasma current, the ECE signal, the intensities added over all pixels of the IR image, the scintillator probe signal, the SXR signal and the Mirnov signal. Dashed lines (a)–(f) correspond to the sub-figures (*a*)–(*f*) in (*A*) and (*B*).

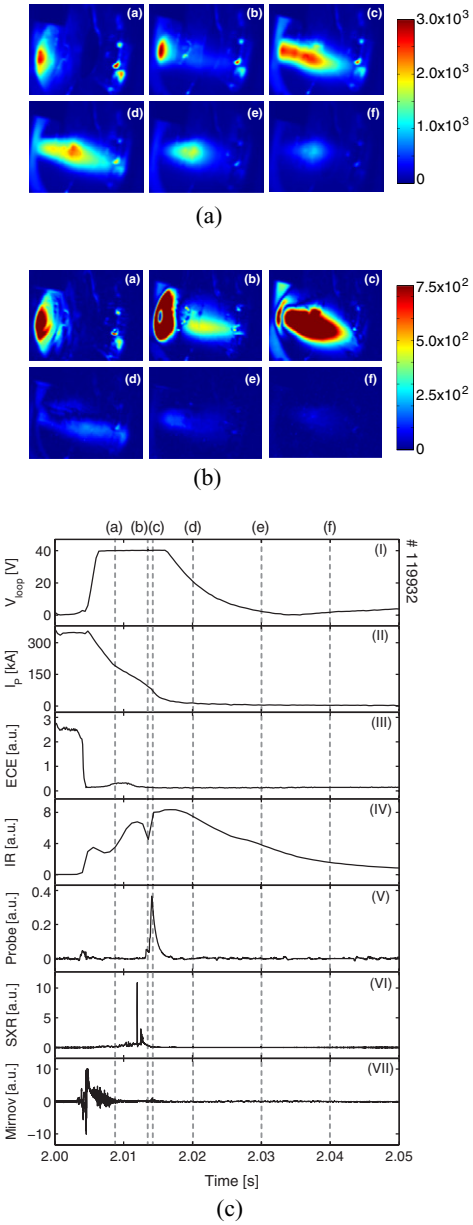

Figure 4. (*A*) IR images observed by the camera and (*B*) the images obtained from subtracting consecutive images for discharge #119932 at (*a*) $t = 2.009$ s, (*b*) $t = 2.013$ s, (*c*) $t = 2.014$ s, (*d*) $t = 2.020$ s, (*e*) $t = 3.030$ s and (*f*) $t = 2.040$ s. (*C*) Temporal evolution of the disruption of discharge #119932: (top to bottom) time trace of the loop voltage, the plasma current, the ECE signal, the intensities added over all pixels of the IR image, the scintillator probe signal, the SXR signal and the Mirnov signal. Dashed lines (a)–(f) correspond to the sub-figures (*a*)–(*f*) in (*A*) and (*B*).

suddenly accompanied by a RE burst, a sharp SXR spike and a Mirnov signal spike (see figures 3(*C*)(V)–(VII) dashed line (f)).

3.3. REs survive the runaway plateau termination

In the third class of observations, the high energy part of the runaway beam survives longer than one expects from the conventional traces such as the plasma current or SXR signals. After the runaway beam is generated and develops at the HFS, it moves more and more towards the HFS due to the positive vertical field (see figures 4(*A*)(*a*) and (*b*)). SXR spikes are present during the runaway plateau phase but no probe signal is observed because in this case the plasma is shifted away from the probe (see figures 4(*C*)(V) and (VI) dashed line (a)). The runaway plateau termination takes place at $t = 2.015$ s. A runaway burst is observed followed by a sudden appearance of the REs at the LFS. In figure 4(*A*)(*c*), it seems like the beam moves rapidly towards the LFS. However, the image obtained

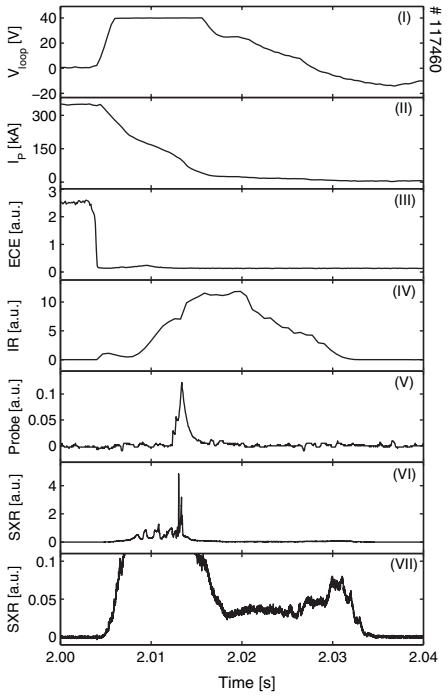

Figure 5. Temporal evolution of the disruption of discharge #117460: (top to bottom) time trace of the loop voltage, the plasma current, the ECE signal, the intensities added over all pixels of the IR image, the scintillator probe signal, the SXR signal and the magnified SXR signal.

from consecutive image subtraction in figure 4(*B*)(*c*) shows that a small amount of REs already exists at the LFS. When the current drops to almost zero these REs as well as the REs which have energies a bit lower than 25 MeV are accelerated and become visible.

Although the plasma current drops to almost zero (see figure 4(*C*)(II)), a significant number of REs can still be confined. The runaway beam then decays gradually over several tens of ms. During this phase neither the SXR nor the probe shows any signal as the loss rate of the REs is too low. The intensity of the runaway beam in this case is much smaller than in previous cases because the runaway plateau phase, in which the REs are accelerated, is much shorter. The REs do not have enough time to gain high energies. In this example, the MHD activity stops at $t \approx 2.014$ s (see figure 4(*B*) dashed line (c)) while the synchrotron radiation continues to be emitted by the REs over a few tens of ms. Observations of significant number of REs after runaway plateau termination have been reported previously [22]. There are other examples where the SXR signal continues when the plasma current has apparently ended, however, with a strongly reduced amplitude. Figure 5 is an example in which the plasma current seems to finish already at $t = 2.015$ s while the IR-synchrotron signal continues for 15 ms. Other characteristic runaway signals like the probe signal and the SXR signal seem to stop with the plasma current at $t = 2.015$ s. However, if the SXR signal is enhanced by a factor of 50, one sees that the signal continues to the end of the IR radiation (see figure 5 (VI)). The presence of the SXR signal at this phase confirms that the REs can survive the runaway plateau termination and can be confined by the plasma current of a few tens of kA.

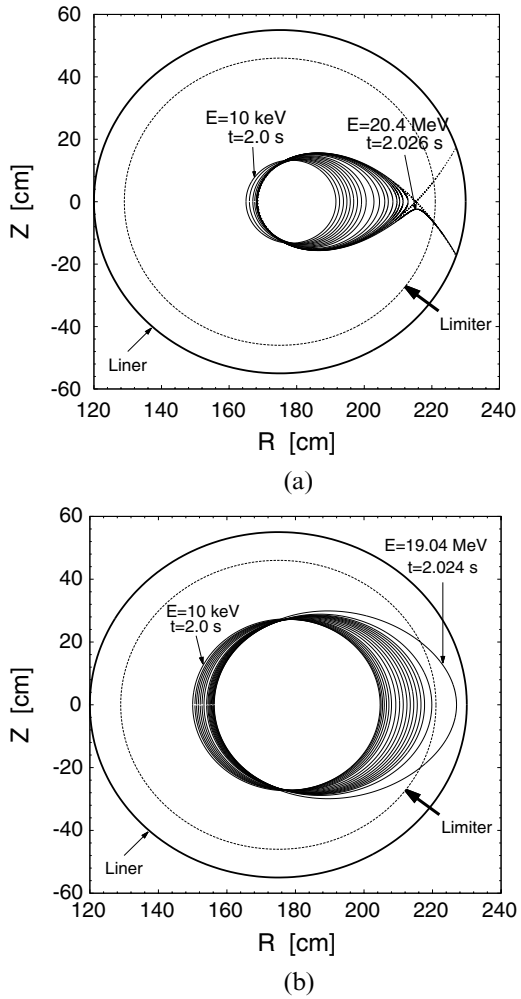

Figure 6. The evolution of the orbits for electrons of discharge #117859 starting at (*a*) $R = 165$ cm and (*b*) $R = 150$ cm.

4. Runaway orbits

Runaway orbits during disruptions are so far calculated for a constant energy. In a new approach, the full orbit development in the given toroidal electric field of the disruption is calculated by a mapping method. Since of course the calculation of the full orbit evolution would be extraordinarily time consuming, smaller parts of the orbit are computed and the evolution extrapolated in the next step followed by another orbit mapping etc.

The method allows for a visualization of the history of the electron acceleration, i.e. which electrons can gain energy and which electrons are lost during the acceleration phase. A typical loop voltage and plasma current are taken from the experiment. Figure 6(*a*) shows the evolution of the orbits for an electron in the core and figure 6(*b*) the orbit more outside. In figure 7 the energy gain of the electrons is shown for electrons of different starting positions; the major radius of the TEXTOR axis amounts to 175 cm. Only the core electrons remain confined throughout the disruption while electrons with $r > a/2 \approx 20$ cm are quickly lost before they gain sufficient energy to emit synchrotron radiation in the operating wavelength range of the camera. In addition, the right axes of figure 7 show the loop voltage and the plasma current; the

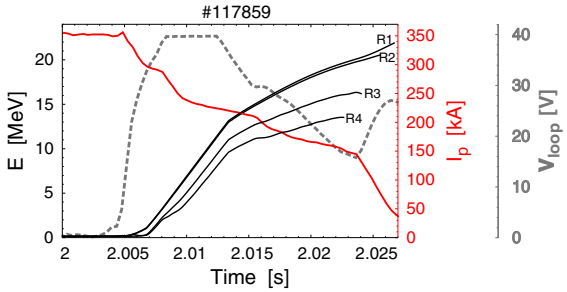

Figure 7. Temporal evolution of the disruption of discharge #117859: energy gain of the electrons starting at $R_1 = 172$ cm, $R_2 = 165$ cm, $R_3 = 150$ cm and $R_4 = 140$ cm (black), the plasma current (red), and the loop voltage (dashed grey).

loop voltage is cut at about 40 V due to the limitation of the data logger. Therefore, the final energy of the core electrons could reach 25 MeV, consistent with the limit required that the synchrotron radiation can be observed. The orbits of the outer electrons clearly hit the wall before they can reach such energies. The energy of about 25 MeV, however, is also the upper limit which is given by $\int E(t)\,\mathrm{d}t$ during the current decay.

The orbit radii remain nearly unchanged but drifts to the LFS as expected. The shift amounts to about $\delta = \frac{\langle q\rangle W}{ecB_\phi}$, where $\langle q\rangle = \langle \frac{r}{B_\theta}\rangle \frac{B_\phi}{R}$, and W the runaway energy. This shift is identical with the shift from the resonant magnetic surface and visualizes the shielding of the runaways from the magnetic perturbation.

If we neglect other boundaries, then the limiting orbit shows an X-point towards the LFS. Beyond the X-point, the orbits are open and the runaways are quickly lost. For a given experiment, it depends on the details of the vessel whether the X-point is the limitation of the runaway orbits or whether it is the orbit shift towards a limiter or the wall which leads to the loss of the runaways. In case of TEXTOR disruptions, both limits are nearly identical.

5. Induced disruptions with runaway mitigation methods applied

The following examples show effects of various mitigation methods on the behaviour of REs during induced disruptions. All disruptions presented in this section are triggered by an argon injection performed by valve 1 at $t = 2$ s. First, valve 2, which is sufficient to remove runaways from a low density runaway discharge, was applied. Then valve 3 capable of a massive gas injection is applied. Finally, the option of runaway removal by ergodization of the magnetic field lines are tested.

5.1. Fast gas injection performed by valve 2

As already discussed above, valve 2 is used because of its ability to suppress REs during low density discharges. The effect of 3 different types of gas puffs, namely helium, neon and argon, on the runaway confinement is investigated. 2.2×10^{22} atoms of gas are injected by valve 2 at different times. In discharge #117535, valve 2 injects 2.2×10^{22} atoms of neon at 15 ms after the first injection. The runaway beam develops at the HFS similarly as in typical induced disruptions. At $t = 2.022$ s the runaway beam expands suddenly and the intensity at the centre of the beam decreases as can be seen in figures 8(A)(b) and 8(B)(b). At this time, a Mirnov signal spike is observed (see figure 8(C)(VII) (black curve) dashed line (b)). As the RE loss is enhanced, the current decay rate increases accompanied by runaway bursts and SXR spikes (see figure 8(C) (black curve)). The IR images in figures 8(A)(c)–(f) show that the beam does not develop further due to the loss. The beam becomes smaller while the intensity at the centre of the beam does not change significantly. At the edge, intensity fluctuations of the beam are observed as shown in figures 8(B)(b)–(f) (white arrows). These fluctuations, which are not present in typical induced disruptions, indicate the perturbations initiated by the gas puff. The SXR signal rises again during the runaway plateau termination but no runaway burst is observed by the scintillator probe. When the plasma is terminated, the REs are lost to the wall and may not hit the probe.

In discharge #117509, 2.2×10^{22} atoms of argon are injected at 15 ms after the first injection. No sudden expansion of the runaway beam is observed. The temporal evolution of the beam is similar to the first case of a typical induced disruption without mode excitation (see figure 9(A)). The runaway beam is generated and develops at the HFS. The beam intensity at the centre increases with time while the beam shrinks. The filamented structures are also present in figure 9(B) which is obtained from consecutive image subtraction. However, the argon injection results in an enhancement of the runaway loss. During the plateau phase, peaks in the SXR are observed. All the REs are lost at 16 ms after the injection. In comparison with the previous example, the runaway confinement time is shorter (see figure 8(C) (red curve) compared with (black curve)). The runaway plateau is terminated ~30 ms earlier. It agrees with the synchrotron radiation observed by IR camera. The effect of argon injection is detected later than that of neon injection because argon needs a longer time to travel from the valve to the plasma.

In figure 10, the averaged runaway plateau lengths of the disruptions mitigated by different types of gas are plotted against a time scale of the discharge, at which valve 2 is triggered. A plateau length is determined from the width of the runaway current, which is obtained by subtracting the exponential current decay from the plasma current. For each condition, we made 2–5 measurements. The data plotted in this figure are obtained by averaging the plateau lengths of all discharges under the same condition. The error bars present the standard deviations.

2.2×10^{22} atoms of argon, neon and helium are injected separately at different times. The earlier the gas is injected, the stronger the effect is obtained. Argon provides the strongest effect. Nevertheless, the effect is not strong enough to effectively suppress the REs. To us the result was a surprise, because the runaways are regularly and quickly expelled from normal runaway discharges. This means obviously the runaways are much more robust in the current decay phase of a disruption than in a normal runaway discharge.

5.2. Argon injection performed by valve 3

Since argon, in comparison with helium and neon, provides the strongest effect on the runaway suppression, this section

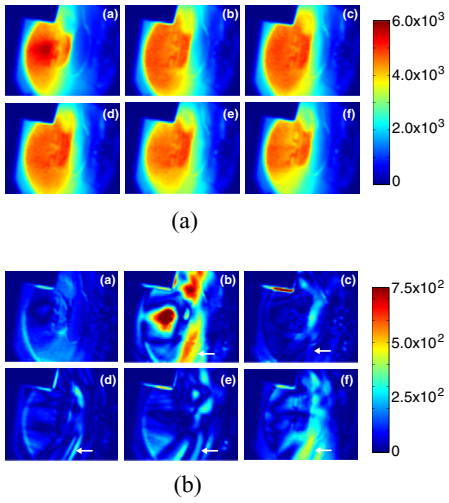

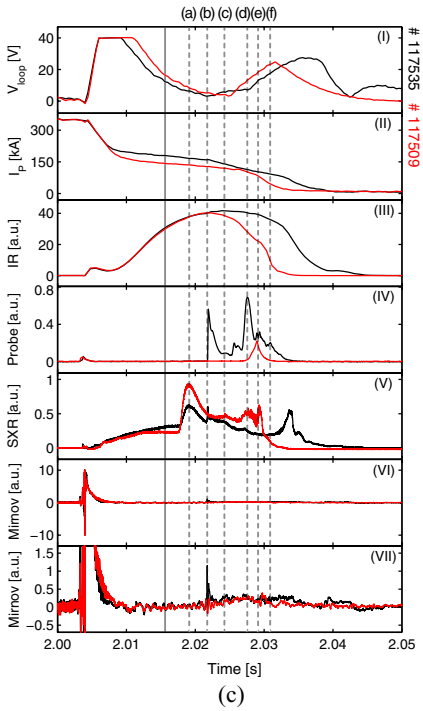

Figure 8. (*A*) IR images observed by the camera and (*B*) the images obtained from subtracting consecutive images for discharge #117535 at (*a*) $t = 2.019$ s, (*b*) $t = 2.022$ s, (*c*) $t = 2.024$ s, (*d*) $t = 2.027$ s, (*e*) $t = 2.029$ s and (*f*) $t = 2.031$ s. White arrows indicate the fluctuations, which are not present in the typical induced disruptions. (*C*) Temporal evolution of the disruption of discharges #117535 (black curve) and #117509 (red curve). In discharge #117535, 2.2×10^{22} atoms of neon are injected at $t = 2.015$ s. In discharge #117509, argon is used instead. A grey line indicates the time at which the gas puffs are injected. Dashed lines (a)–(f) correspond to the sub-figures (*a*)–(*f*) in figures 8(*A*), 8(*B*), 9(*A*) and 9(*B*).

focuses only on the influence of an argon puff injected by valve 3 on runaway mitigation. Up to 5.3×10^{22} atoms of argon are injected at different times. In discharge #119989, 1.3×10^{22} atoms of argon are injected at $t = 2.004$ s. The runaway beam evolves and remains at the HFS. In comparison with typical induced disruptions, the beam develops more slowly. At $t = 2.011$ s, a SXR and a Mirnov signal spikes are present

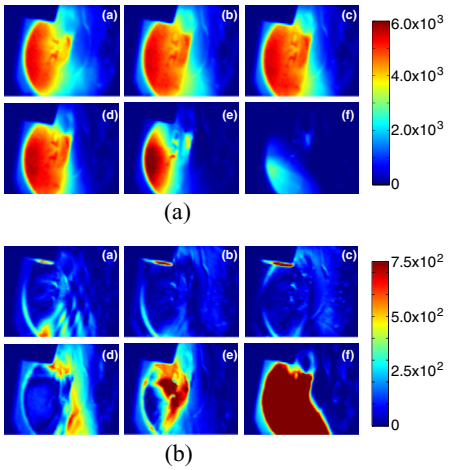

Figure 9. (*A*) IR images observed by the camera and (*B*) the images obtained from subtracting consecutive images for discharge #117509 at (*a*) $t = 2.019$ s, (*b*) $t = 2.022$ s, (*c*) $t = 2.024$ s, (*d*) $t = 2.027$ s, (*e*) $t = 2.029$ s and (*f*) $t = 2.031$ s.

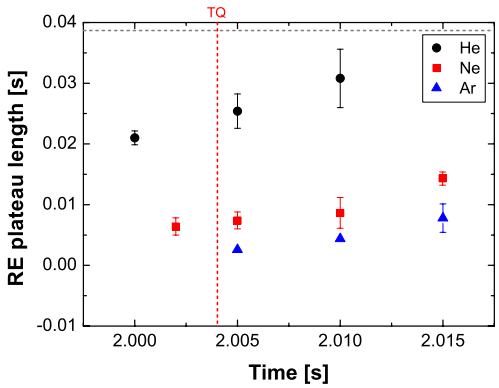

Figure 10. Averaged runaway plateau length of the induced disruptions mitigated by gas puffs of helium (black), neon (red) and argon (blue). 2.2×10^{22} atoms of gas are injected by valve 2 at different times. The x-axis indicates the time when valve 2 is triggered. A grey dashed line presents an averaged plateau length of typical induced disruptions and a red dashed line the TQ time.

as shown in figures 11(*C*) dashed line (a). The intensity of the runaway beam at the centre increases suddenly (see figures 11(*A*)(*a*) and (*B*)(*a*)). However, the radius of the beam does not change significantly. After that only small Mirnov oscillations are observed. Neither the SXR spike nor the probe signal is present. REs are well confined within the plasma. A small fluctuation of the runaway beam intensity is observed 10 ms after the fast argon injection (see figures 11(*B*)(*b*) and (*c*)). As the runaway plateau is terminated, the plasma current drops to almost zero and the REs suddenly appear at the LFS. It is still not clear whether the REs observed at the LFS afterwards are the existing REs which move suddenly towards the LFS or a new population of REs develops at the LFS. Some discharges seem to favour the first scenario and others the alternative (see subsection 3.3). The runaway burst and the SXR spike at the runaway plateau termination indicate the runaway loss (see figures 11(*C*)(IV) and (V) dashed line (e)). However, a significant number of the REs survives as presented in figure 11(*C*)(III) (black curve). The beam remains visible over 5 ms and the SXR signal decays slowly to zero.

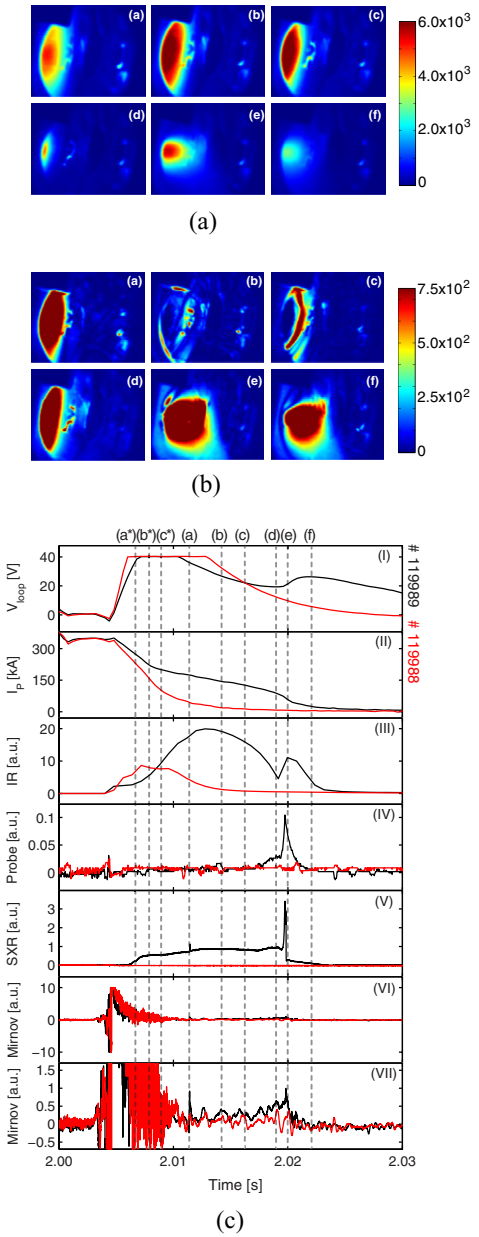

Figure 11. (*A*) IR images observed by the camera and (*B*) the images obtained from subtracting consecutive images for discharge #119989 at (*a*) $t = 2.011$ s, (*b*) $t = 2.014$ s, (*c*) $t = 2.016$ s, (*d*) $t = 2.019$ s, (*e*) $t = 2.020$ s and (*f*) $t = 2.022$ s. (*C*) Temporal evolution of the disruption of discharge #119989 (black) and discharge #119988 (red), in which 1.3×10^{22} atoms of argon are injected at $t = 2.004$ s and $t = 2.003$ s, respectively. The lowest sub-figure presents the magnified Mirnov signal. Dashed lines (a*)–(c*) correspond to the sub-figures (*a*)–(*c*) in figure 12. Dashed lines (a)–(f) correspond to the sub-figures (*a*)–(*f*) in (*A*) and (*B*).

The disruption of discharge #119988 is runaway free. In this discharge, 1.3×10^{22} atoms of argon are injected at $t = 2.003$ s. The probe and the SXR signal are zero. Additionally, neither synchrotron radiation emitted by the REs nor the runaway plateau is observed. The IR peak presented in figure 11(*C*)(III) (red curve) is IR emitted by the injected gas and thermal radiation originating from the wall, which is heated during the TQ (see figure 12). The IR radiation originates from a neutral gas is very diffuse. This means that

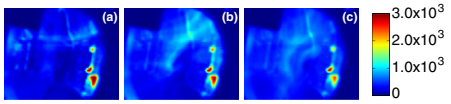

Figure 12. IR radiation observed by the camera of discharge #119988 at (*a*) $t = 2.007$ s, (*b*) $t = 2.008$ s, (*c*) $t = 2.009$ s. The IR observed here is emitted by the injected gas and is the thermal radiation from the heated wall.

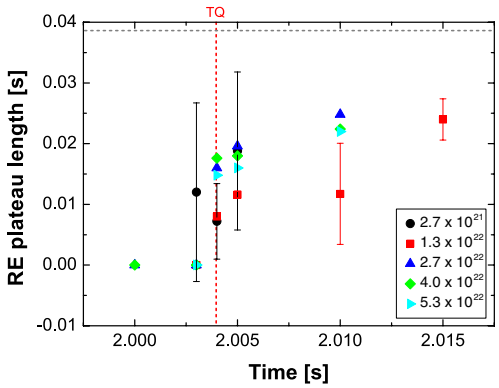

Figure 13. Averaged runaway plateau length of the induced disruptions mitigated by argon puff: 2.7×10^{21} atoms (black), 1.3×10^{22} atoms (red), 2.7×10^{22} atoms (blue), 4.0×10^{22} atoms (green), 5.3×10^{22} atoms (light blue). Gas puffing is performed by valve 3. The x-axis indicates the time when valve 3 is triggered. A grey dashed line presents an averaged plateau length of typical induced disruptions and a red dashed line the TQ time. The large error bars are caused by the strong deviation of the plateau lengths of some shots from the average values.

the gas injection of valve 3 suppresses the runaway generation completely. However, a later argon injection into a disruption with already existing REs does not eliminate them.

Similar to the effect of the gas puff (valve 2), if the gas is injected earlier, the effect is stronger (see figure 13). Since valve 3 is located as close to the plasma as possible (closer than valve 2), the gradient of the gas flow hitting the plasma surface is higher than with valve 2. In addition, the area of orifice diameter is twice as large as the one of valve 2. The injected gas, therefore, penetrates deeper into the plasma. The runaway-free disruptions are achieved when $\geqslant 1.3 \times 10^{22}$ atoms of argon are injected at $\leqslant 3$ ms after the disruption is triggered. The effect of the argon puff decreases drastically if the gas is injected after the TQ.

5.3. Dynamic ergodic divertor (DED) 6/2 mode

In discharge #120103 (figure 14), the DED is applied in the 6/2 mode at $t = 2.00$ s (at the same time as the argon is injected by valve 1). Because of its substantial inductivity, the rise time of the DED current amounts to about 60 ms. Therefore, the current is not constant during the disruption, unless it is switched on prior to the disruption. In this case, REs are also generated at the HFS. However, the runaway beam develops more slowly in comparison with typical induced disruptions. The runaway beam is broadened. REs are then lost to the LFS and hit the probe. IR radiation at the probe position is present at the very beginning of the disruption as shown in figure 14(*A*) (white rings). The IR intensity at the probe position increases with time, i.e. REs are lost continuously. The runaway plateau

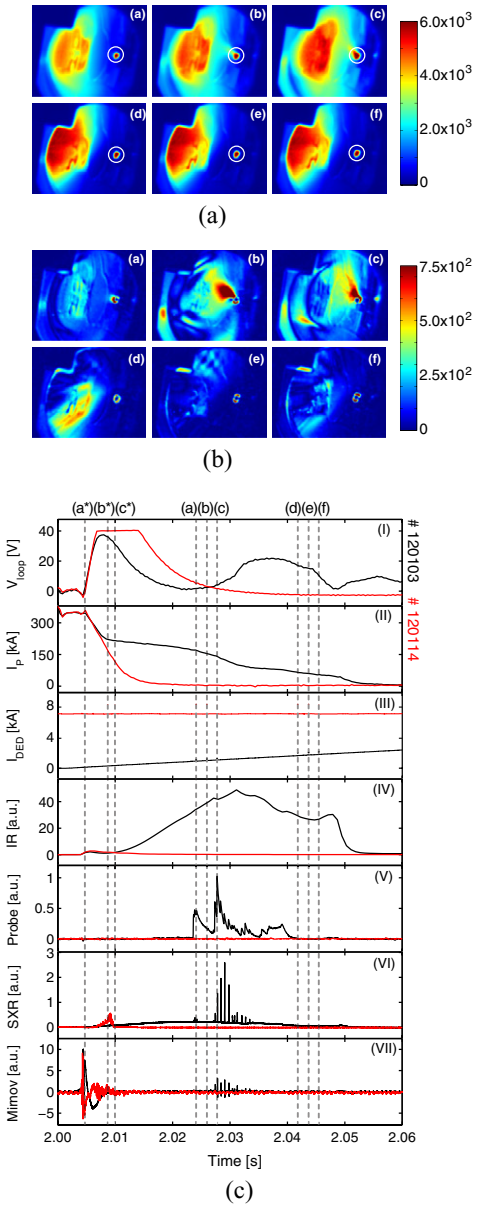

Figure 14. (*A*) IR images observed by the camera and (*B*) the images obtained from subtracting consecutive images for discharge #120103 at (*a*) $t = 2.023$ s, (*b*) $t = 2.025$ s, (*c*) $t = 2.027$ s, (*d*) $t = 2.042$ s, (*e*) $t = 2.044$ s and (*f*) $t = 2.046$ s. White rings indicate the scintillator probe tip. (*C*) Temporal evolution of the disruption of discharge #120103 (black) and discharge #120114 (red), in which the DED current of 7 kA is applied on at $t = 2.00$ s and $t = 1.70$ s, respectively. The DED currents are shown in sub-figure (III). Dashed lines (a*)–(c*) correspond to the sub-figures (*a*)–(*c*) in figure 15. Dashed lines (a)–(f) correspond to the sub-figures (*a*)–(*f*) in (*A*) and (*B*).

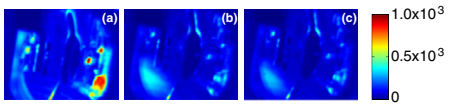

Figure 15. IR radiation observed by the camera of discharge #120114 at (*a*) $t = 2.005$ s, (*b*) $t = 2.009$ s, (*c*) $t = 2.010$ s.

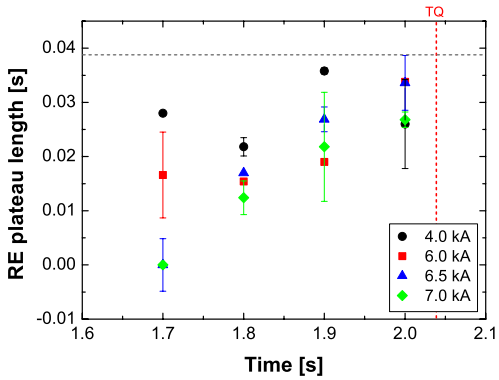

Figure 16. Averaged runaway plateau length of the induced disruptions mitigated by the DED 6/2 mode. DED currents of 4 kA (black), 6 kA (red), 6.5 kA (blue) and 7 kA (green) are applied (separately) at different times. The x-axis indicates the time when the DED is applied. A grey dashed line presents an averaged plateau length of typical induced disruptions and a red dashed line the TQ time.

termination takes place at $t = 2.05$ s accompanied by a sudden loss of REs. The intensity profile of the runaway beam is affected by the applied DED. It is no longer smooth as shown in figure 14(*B*). In contrast to the previous cases of gas injection, the filamentary structure is observed not only at the edge of the beam but also in the beam centre. It is most likely that the 'filamentary structure' originates from the modes which are induced by the external DED field.

The time traces of the loop voltage, the plasma current, the DED current, the intensities added over all pixels of the IR image, the scintillator probe signal, the SXR signal and the Mirnov signal of the discharge #120103 are shown in figure 14(*C*) (black curve). As the DED current reaches 1 kA at $t \approx 2.03$ s, a small-stepwise reduction of plasma current is observed (see figure 14(*C*)(II) dashed line (d)). Additionally, RE bursts, SXR and Mirnov signal spikes are present. The intensity of the runaway beam decreases while the IR intensity at the probe tip increases. Therefore, the intensity added over all pixels of the IR image decreases slightly. The runaway beam moves a little towards the LFS at $t = 2.047$ s. Since a larger area of the beam is in the camera's field of view, the intensity added over all pixels of the IR image increases. The intensity of the runaway beam, in contrast, continues to decrease. The DED leads to REs loss before REs gain high energies. However, a significant number of REs is still confined in the plasma.

In the discharge #120114, the DED is switched on at $t = 1.70$ s. The DED current reaches the maximum value of 7 kA at $t = 1.90$ s. The runaway beam develops and remains at the HFS. The beam does not touch the probe, therefore, no probe signal is present (see figure 14(*C*)(IV) (red curve)). Although no runaway plateau is present, a small number of REs is observed by the IR camera as can be seen in figure 15. Additionally, the SXR signal is also present. However, REs are lost rapidly shortly after the TQ. It is shown in figure 16 that the earlier the DED is switched on, the stronger the effect on REs suppression is obtained. The impact on the RE confinement in discharges, in which the DED is applied at $t = 1.70$ s, is much stronger than in case where the DED is applied at $t = 1.80$ s although the DED current of both cases are the same, i.e. 7 kA, when the argon puff is injected.

In order to obtain a significant effect of the DED on the RE confinement, the DED has to be applied at least 0.3 s

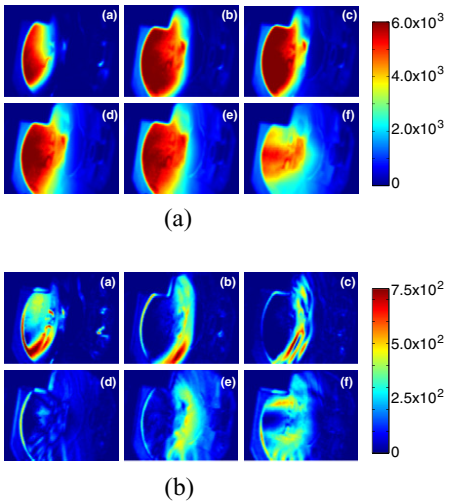

Figure 17. (*A*) IR images observed by the camera and (*B*) the images obtained from subtracting consecutive images for discharge #119889 at (*a*) $t = 2.015$ s, (*b*) $t = 2.026$ s, (*c*) $t = 2.033$ s, (*d*) $t = 2.047$ s, (*e*) $t = 2.050$ s and (*f*) $t = 2.063$ s. Here, the DED current of 1 kA is applied at $t = 1.82$ s.

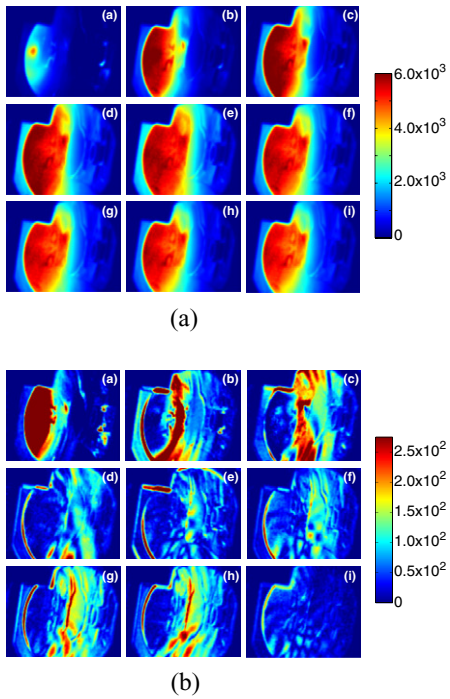

Figure 18. (*A*) IR images observed by the camera and (*B*) the images obtained from subtracting consecutive images for discharge #119869 at (*a*) $t = 2.013$ s, (*b*) $t = 2.022$ s, (*c*) $t = 2.033$ s, (*d*) $t = 2.045$ s, (*e*) $t = 2.065$ s, (*f*) $t = 2.080$ s, (*g*) $t = 2.085$ s, (*h*) $t = 2.087$ s and (*i*) $t = 2.091$ s. Here, the DED current of 1 kA is applied at $t = 2.01$ s.

before the disruption takes place. Otherwise the effect is minor as can be seen in figure 16. This method is rather impractical for disruption mitigation since a disruption is a transient event and the method that provides a fast response is required. Additionally, complete runaway suppression cannot be achieved. Although the perturbations generated by the DED, in comparison with the case of the gas puff, can penetrated deeper into the runaway beam, it is not strong enough to eject all REs from the plasma.

5.4. Dynamic ergodic divertor (DED) 3/1 mode

The influence of the resonant magnetic perturbation (RMP) produced by the DED 3/1 mode on the runaway suppression in the TEXTOR tokamak has been investigated by Lehnen [20] and Koslowski [31]. It has been shown in [20] that the loss rate of REs is significantly enhanced if sufficiently strong RMPs with $n = 1, 2$ are applied. However, a complete runaway suppression cannot be achieved. The experimental results in [31] shows, conversely, no clear effect of the RMPs on the runaway suppression. Here we will discuss only the results observed by the IR camera.

Figure 17, shows the temporal evolution of the runaway beam of discharge #119889, in which the DED current of 1 kA is applied at 1.82 s. The DED is constant during the whole disruption. The fluctuation of the beam intensity distribution as present in the case of the gas puff injection (valve 2) is observed (see figures 17(*A*) and (*B*)). However, the perturbations penetrate deeper into the runaway beam than the perturbations initiated by the gas puff (valve 2). A different runaway behaviour is found in discharge #119869, in which the DED is applied at $t = 2.01$ s, i.e. after the disruption is triggered. The RE confinement is improved. A runaway is confined longer in the plasma than in the previous case. Figure 18(*A*) shows that the runaway beam changes only slightly over a long period of time. No sudden loss is observed. In this discharge, different structures are observed as shown in figure 18(*B*). At the beginning of the discharge structures are present only at the edge of the runaway beam. As the perturbations penetrate deep into the beam centre, the intensity of the beam starts to decrease.

It is still not clear whether a tearing mode is also induced if the DED is applied during the disruption. In any case, one finds a rich 'filamentary' structure in particular in the different sequence of figure 18(*B*); the structure reaches deep into the runaway beam as one might expect for the $m/n = 3/1$ mode. This structure could either result from the external ergodization of the DED or the internal ergodization by the mode.

6. Summary and conclusions

In order to study the development of runaway electrons in disruptive discharges, a massive gas injection of argon is applied by valve 1. Key diagnostics are IR-synchrotron radiation measurements for the high energy runaway component ($E > 25$ MeV) and a runaway probe in particular for the runaways with energies of a few MeV up to 22 MeV. The disruption starts with the TQ and an initial exponential decay of the plasma current which is then followed by a characteristic plateau phase in which the runaway beam develops and a runaway plateau termination phase.

Even though the experimental conditions are identical, the runaways can show a quite different time evolution. In the simplest case, the disruption is 'smooth' without mode excitation. A runaway beam with a diameter of about one half of the original plasma diameter develops. The beam size agrees well with the one that is obtained from modelling [22]. In other cases, MHD activity is observed during the plateau

phase. Even though the plasma current shows typical decay steps during this phase, the synchrotron image shows neither special structures in the image of the high energy electrons nor a strong loss. On the contrary, the synchrotron radiation can even still increase. The reason is most likely that low and high energy runaways are not influenced in the same way by MHD perturbations. The orbit of the low energy runaways shows only a small displacement and is close to 'its' resonant magnetic surface and much more perturbed than the high energy ones which have strongly displaced orbits. The high energy runaways are thus shielded from perturbations. Therefore, the loss of the low energy runaway electrons is substantially higher than that of the high energy ones. Since the high energy runaways are confined for a relatively long time in the plasma they can gain more energies and may cause the severe damage to the PFCs when they are lost. Nevertheless, the runaway confinement time depends also on the starting position of the REs. The REs at the core remain confined throughout the disruption while the REs in the outer part are quickly lost because their orbits intersect the limiter or wall. Sometimes, a runaway loss channel towards the wall is observed.

Additionally, we have observed cases, in which the high energy runaways seemed to survive longer than the plasma current. A very low current of between 10 and 20 kA is, in agreement with modelling [22], sufficient to confine 25 MeV runaway electrons. The low current indicates that again the high energy component of the runaways can survive magnetic perturbations and can remain dangerous, in particular for fusion devices, even in late times of the disruption.

Various methods were applied in order to mitigate the effect of the REs. The runaway loss was expected to be initiated by the applied mitigation method and the REs should be lost before they have time to gain high energy. The argon injection performed by valve 3 provides the best results. A complete runaway suppression can be achieved if a moderate amount of gas is injected early enough, i.e. as close as possible to the first injection performed by valve 1 initiating the disruption. Otherwise the mitigation effect is minor. The ergodization during the disruption helps slightly to shorten the runaway confinement time. This indicates that the runaways created during disruptions are very robust, much more than in a low density runaway discharge.

In summary:

- High energy runaways are more difficult to remove than low energy runaways.
- Runaways generated during disruptions are rather robust against attempts to remove them. Fast gas injection and ergodization are effective only if they are applied as close as possible to the first valve trigger and with a large number of injected atoms or with the highest ergodization amplitude available.
- To our experience runaways generated during disruptions can be avoided by either a fast and massive argon injection of the order of 10^{22} atoms (TEXTOR) or by a pre-existing $m/n = 2/1$ tearing mode.

Acknowledgments

This work was supported by the Royal Thai Government, a Jülich R&D contract, the Trilateral Euregio Cluster (TEC) and the DFG program GRK 1203. The authors would like to thank Dr H.R. Koslowski, M. Forster, M. Rack, Dr O. Schmitz and the TEXTOR Team for their support.

References

[1] Schüller F.C. 1995 *Plasma Phys. Control. Fusion* **37** A135
[2] Neyatani Y. *et al* 1999 *Nucl. Fusion* **39** 559
[3] Pautasso G. *et al* 1996 *Nucl. Fusion* **36** 1291
[4] Yoshino R. *et al* 1997 *Plasma Phys. Control. Fusion* **39** 313
[5] Taylor P.L. *et al* 1999 *Phys. Plasmas* **6** 1872
[6] Timokhin V.M. *et al* 2001 *Tech. Phys. Lett.* **27** 795
[7] Whyte D.G. *et al* 2002 *Phys. Rev. Lett.* **89** 055001
[8] Hollman E.M. *et al* 2005 *Nucl. Fusion* **45** 1046
[9] Lehnen M. *et al* 2011 *J. Nucl. Fusion* **51** 123010
[10] Pautasso G. *et al* 2009 *Plasma Phys. Control. Fusion* **51** 124056
[11] Whyte D.G. *et al* 2003 *J. Nucl. Mater.* **313** 1239
[12] Reux C. *et al* 2010 *Nucl. Fusion* **50** 095006
[13] Bakhtiari M. *et al* 2002 *Nucl. Fusion* **42** 1197
[14] Bozhenkov S.A. *et al* 2008 *Plasma Phys. Control. Fusion* **50** 105007
[15] Plyusnin V.V. *et al* 2006 *Nucl. Fusion* **46** 277
[16] Chen Z.Y. *et al* 2013 *Plasma Phys. Control. Fusion* **55** 035007
[17] Martin-Solis J.R. *et al* 1995 *Phys. Plasmas* **6** 238
[18] Hender T.C. *et al* 2007 *Nucl. Fusion* **47** S128–202
[19] Finken K.H. *et al* 2001 *Nucl. Fusion* **41** 11
[20] Lehnen M. *et al* 2008 *Phys. Rev. Lett.* **100** 55003
[21] Kudyakov T. *et al* 2012 *Nucl. Fusion* **52** 023035
[22] Wongrach K. *et al* 2014 *Nucl. Fusion* **54** 043011
[23] Kudyakov T. *et al* 2008 *Rev. Sci. Instrum.* **79** 10F126
[24] Savtchkov A. *et al* 2002 *Rev. Sci. Instrum* **70** 3490
[25] Finken K.H. *et al* 2008 *Nucl. Fusion* **48** 115001
[26] Finken K.H. *et al* 2003 *J. Nucl. Mater.* **313–316** 1247
[27] Finken K.H. *et al* 2011 *Nucl. Fusion* **51** 033007
[28] Lehnen M. *et al* 2009 *J. Nucl. Mater.* **390** 740
[29] Finken K.H. *et al* 2005 *The Structure of Magnetic Field in the TEXTOR-DED: Energy Technology* vol 45 (Jülich: Forschungszentrum Jülich)
[30] Koslowski H.R. *et al* 2006 *Nucl. Fusion* **46** L1
[31] Koslowski H.R. *et al* 2014 *41st EPS Conf. on Plasma Physics* P 5.028 http://ocs.ciemat.es/EPS2014PAP/pdf/P5.028.pdf